Vortex Structure and Evolution within Bow Echoes. Part I: Single-Doppler and Damage Analysis of the 29 June 1998 Derecho

Nolan T. Atkins and Justin M. Arnott[*]

Lyndon State College, Lyndonville, Vermont

Ron W. Przybylinski

National Weather Service, Saint Charles, Missouri

Ray A. Wolf

National Weather Service, Davenport, Iowa

Bradley D. Ketcham[+]

National Weather Service, Lincoln, Illinois

ABSTRACT

Single-Doppler radar along with damage observations are examined to investigate the structural evolution of vortices observed within the 29 June 1998 derecho event that propagated through southeastern Iowa into central and eastern Illinois. A total of 13 meso-γ-scale vortices observed primarily at low levels (0–3 km AGL) along the leading edge of the convective system were detected by the Weather Surveillance Radar-1988 Doppler (WSR-88D) radars at Davenport, Iowa, and Lincoln, Illinois. All but one of the vortices formed after the system evolved into a bow echo. Ten of the vortices formed north of the apex while three formed south of the apex. Seven of the vortices produced tornadoes that created F0–F1 surface damage. None of the vortices exhibited appreciable upscale growth. Careful analysis of the radar data suggests that it may be possible to discern between the tornadic and nontornadic vortices. The tornadic vortices tended to be stronger, longer-lived, and deeper than their nontornadic counterparts. The forecasting implications of these findings are discussed.

Single-Doppler radar observations documenting the evolution of midlevel (3–7 km AGL) "bookend" vortices associated with two embedded bow echoes are also presented. The first pair of midlevel vortices formed approximately 20 min after the time that the larger-scale convective system began its transition into a bow echo, had a lifetime of about 30 min, and was observed north of the primary bow apex. A second embedded bow echo formed approximately 20 min after the first, again north of the primary bow apex. The cyclonic member of this second embedded bow echo grew upscale and eventually became the dominant northern line-end vortex of the convective system. There appears to be no significant relationship or interaction between the low-level and midlevel vortices observed with this case.

1. Introduction

Bow echoes are a well-known, unique form of convective organization that often produce severe weather, especially damaging straight-line winds and tornadoes. Early studies of conventional radar data by Nolen (1959)

and Hamilton (1970) showed that within squall lines, damaging straight-line winds and tornadoes often occur in locations where the radar echoes form a wavelike pattern or bulge. This radar echo configuration was termed the line echo wave pattern (LEWP) by Nolen (1959). Fujita (1978) put forth the first detailed morphological description of this type of radar echo pattern, which he called the "bow echo." His well-known conceptual model shows how an initial tall echo transforms into a bow-shaped line of convective cells as strong downburst winds descend to the surface. At the time of strongest surface winds, a spearhead echo (Fujita and Byers 1977) may form. The system then evolves into a comma-shaped echo as the overall strength of the system declines. Early damage surveys of bow echo events by

---

* Current affiliation: The Pennsylvania State University, University Park, Pennsylvania.

[+] Current affiliation: National Weather Service, Wichita, Kansas.

Corresponding author address: Dr. Nolan T. Atkins, Department of Meteorology, Lyndon State College, 1001 College Road, Lyndonville, VT 05851.
E-mail: nolan.atkins@lyndonstate.edu

Fujita (1978) clearly showed long, narrow swaths of straight-line wind damage generally collocated with the apex of the bow and largely F0–F2 (Fujita 1981) in intensity.

Fujita's damage surveys also confirmed the existence of tornadic damage within bow echoes. The tornadoes produced damage pathlengths generally less than 20 km and F0–F1 damage. Subsequent observational studies (e.g., Forbes and Wakimoto 1983; Wakimoto 1983; Przybylinski 1988, 1995; DeWald et al. 1998; Howieson and Tipton 1998; Funk et al. 1999; Arnott and Atkins 2002) have since corroborated Fujita's findings, documenting cyclonic tornadoes occurring within bow echoes that produce relatively short damage tracks of F0–F2 damage intensity at or north of the bow echo apex. Observations by Forbes and Wakimoto (1983), Smith and Partacz (1985), Przybylinski (1988), and Pence et al. (1998), however, have shown that bow echo tornadoes are capable of producing up to F3 damage, while Wakimoto (1983) documented an F4 anticyclonic tornado located in the cyclonic shear region north of the bow apex. The mechanisms responsible for tornadogenesis within bow echoes are still not well understood.

With the installation of the Weather Surveillance Radar-1988 Doppler (WSR-88D) radars in the late 1980s and 1990s, more frequent high-resolution radar observations of the parent circulations producing bow echo tornadoes (hereafter referred to as mesovortices) have been made. Many studies (e.g., Burgess and Smull 1990; Przybylinski 1995; Przybylinski et al. 1996; Spoden et al. 1998; DeWald et al. 1998; Funk et al. 1999; Arnott and Atkins 2002; Wolf 2002) have shown that these circulations are often 1) observed at low levels (generally below 3 km) and are not associated with significant midlevel rotation, 2) formed at the leading edge of the bow echo along a horizontal gradient in radar reflectivity, 3) have lifetimes of an hour or less, and 4) have horizontal dimensions that are meso-γ (2–20 km) in scale (Orlanski 1975).

While these studies have shown that the mesovortices tend to form at or north of the bow echo apex, they have also been observed at the intersection point of the primary convective system with a preexisting boundary (Schmocker et al. 2000; Przybylinski et al. 2000; DeWald and Funk 2000; Arnott and Atkins 2002; Wolf 2002). The preexisting boundary is often a stationary or warm front or outflow boundary oriented nearly perpendicular to the primary convective system. Bow echo tornadoes can also form in close proximity to the northern cyclonic member of the "book end" vortices (Pfost and Gerard 1997; Howieson and Tipton 1998). The bookend (Weisman 1993) vortices are a fundamental system-scale (tens of kilometers) feature of a bow echo and form at midlevels (3–7 km AGL) behind the leading edge of the convective system, often embedded within precipitation. Their genesis has been attributed to the vertical tilting of baroclinically generated horizontal

vorticity by the system-scale updraft along the gust front (Weisman and Davis 1998).

Unfortunately, the aforementioned observational studies have not been able to examine the genesis mechanisms of the mesovortices largely because of radar sampling limitations and the lack of high-resolution thermodynamic observations near bow echoes. Recent idealized numerical simulations by Weisman and Trapp (2003) suggest that mesovortices readily form within bow echoes when the environmental wind shear magnitude is greater than 15 m s^{-1} or more over the lowest 2.5 km. Weaker, shorter-lived vortices, however, are formed within bow echoes in weaker sheared environments. The genesis of these circulations is attributed to the tilting of crosswise horizontal baroclinic vorticity by downdrafts at low levels (Trapp and Weisman 2003). Stretching of planetary vorticity further amplifies the positive vertical vorticity over time.

The small scale, short lifetimes, and lack of well-defined radar-detected precursors to mesovortex genesis make detection and warning of tornadic activity within bow echoes challenging. According to Tessendorf and Trapp (2000), tornadoes formed within squall lines and bow echoes represent a nonnegligible number of the total tornadoes formed nationwide, estimated to be 20%. This problem is further compounded by the fact that not all of the mesovortices formed at the leading edge of bow echoes are tornadic (e.g., Funk et al. 1999; Arnott and Atkins 2002). The differences in structure and evolution between tornadic and nontornadic mesovortices within bow echoes have not been documented in the literature.

In addition to their possible association with tornadoes, bookend vortices have been shown to enhance the rear-inflow jet circulation by as much as 30%–50% (Weisman 1993). Furthermore, Weisman and Trapp (2003) suggest a close relationship between the bookend vortices and the low-level mesovortices. When the low-level environmental shear is large, upscale growth of the low-level mesovortices into line-end vortices is simulated. While single-Doppler radar observations have documented the structural evolution of the low-level mesovortices formed on the leading edge of bow echoes, the same cannot be said for the midlevel bookend vortices. In fact, the authors are unaware of any observational study that documents the genesis and subsequent evolution of the bookend vortices.

On 29 June 1998, a line of hybrid supercells originating over northeast Nebraska moved along a stationary front into central Iowa and subsequently evolved into a bow echo as the convective system moved southeastward into northwest Illinois (Wolf 2000; Arnott and Atkins 2002). This quasi-linear convective system (QLCS) met the derecho criteria put forth by Johns and Hirt (1987). It has been shown that this area of the Midwest is a climatologically favored area for derecho development during the summer months (Johns and Hirt 1987; Bentley and Mote 1998). A total of 13 meso-

vortices were observed in the Davenport, Iowa (KDVN), and Lincoln, Illinois (KILX), single-Doppler radar data along the leading edge of the convective system. Seven of the circulations produced F0–F1 tornadoes.

In this two-part paper, the genesis and structural evolution of the observed mesovortices are investigated through a combination of detailed radar and damage analyses in Part I and numerical simulation of the 29 June 1998 event in Part II. The specific objectives of Part I are to document the structural evolution of the observed mesovortices with emphasis on the differences between the tornadic and nontornadic vortices. Second, the structural evolution of midlevel bookend vortices associated with two embedded bow echoes are documented with single-Doppler radar observations. In Part II of this paper, numerical simulations from the Weather Research and Forecast (WRF) model (Skamarock et al. 2001) of the 29 June 1998 event will be presented. The simulations will be diagnosed to examine the genesis mechanisms and evolution of the mesovortices formed within the simulated bow echo.

In section 2, the synoptic-scale environment for 29 June 1998 is discussed. A satellite analysis is presented in section 3. Sections 4 and 5 illustrate the system-scale features and damage analyses of the 29 June 1998 derecho, respectively. Finally, section 6 presents observations of the mesovortices and embedded bookend vortices, and conclusions are discussed in section 7.

2. Synoptic-scale environment on 29 June 1998

The synoptic-scale environment observed on 29 June 1998 over the midwestern portion of the United States was very consistent with the warm-season "progressive" type II derecho environment described by Johns and Hirt (1987). This environment is characterized by relatively weak synoptic-scale forcing producing northwesterly flow at 500 mb, advection of relatively warm, moist air at 850 mb in the vicinity of the derecho initiation area, and a stationary thermal-moisture boundary at the surface that is oriented in the west–east direction. The environment is also characterized by strong instability and moderate low-level unidirectional shear. The derecho initiates along the thermal boundary and subsequently moves along it with some component of motion directed into the warm sector.

A surface analysis at 1200 UTC on 29 June 1998 is shown in Fig. 1. Prominent is a stationary front oriented west–east across the northern portion of Iowa. Superimposed reflectivity data show that the derecho initiates near the thermal boundary and subsequently moves southeastward into the warm sector, consistent with the results of Johns and Hirt (1987). Warm, moist southerly flow is evident south of the front. An 1800 UTC sounding (Fig. 2) launched at Lincoln, Illinois, shows that large convective instability along with strong low and midlevel unidirectional shear were present over central Illinois. Previous modeling and observational studies
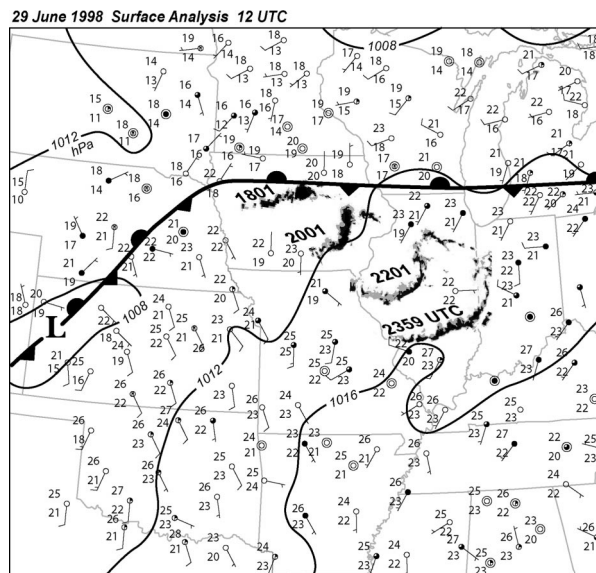

Fig. 1. Surface analysis on 29 Jun 1998 at 1200 UTC. Solid lines are isobars contoured every 4 hPa. Radar reflectivity data from the Davenport, IA, and Lincoln, IL, WSR-88Ds at 1801, 2001, 2201, and 2359 UTC on 29 Jun 1998 are superimposed on the surface data. Winds are shown in meters per second (half barb = 2.5 m s⁻¹; full barb = 5.0 m s⁻¹). Temperature and dewpoint are also shown in degrees Celsius.

(e.g., Johns and Hirt 1987; Weisman 1993; Evans and Doswell 2001) have shown that derecho-producing environments are characterized by large convective instability and moderate to strong low-level shear. The 0–2.5-km shear vector was oriented to the southeast at 120°, consistent with the system motion of 31.2 m s⁻¹ at 115° (Fig. 1). Also noteworthy in the sounding data is the presence of relatively dry air at midlevels.

At 850 hPa (Fig. 3a), strong southwesterly flow in advance of a trough is observed over the southern plains extending northward into southern Nebraska and Iowa. Prominent thermal advection by the southwesterly flow is evident within the derecho-initiation area of central Iowa and has transported air with temperature and equivalent potential temperature values in excess of 20°C and 345 K, respectively, into southern Iowa. At 500 hPa (Fig. 3b), moderate west-northwest flow and broad diffluence is observed over Iowa. Consistent with the results of Johns (1993), the derecho initiated south of the 500-mb jet axis that is located over southern Minnesota in Fig. 3b.

3. Satellite analysis

A more detailed depiction of the mesoscale environment along with the initiation and subsequent evolution of the derecho is shown in Fig. 4. At 1615 UTC (Fig. 4a), remnant convection is observed over southern Minnesota and northern Iowa that has produced a southeastward-moving outflow boundary located just north of the stationary front. Only weak convection is ob-
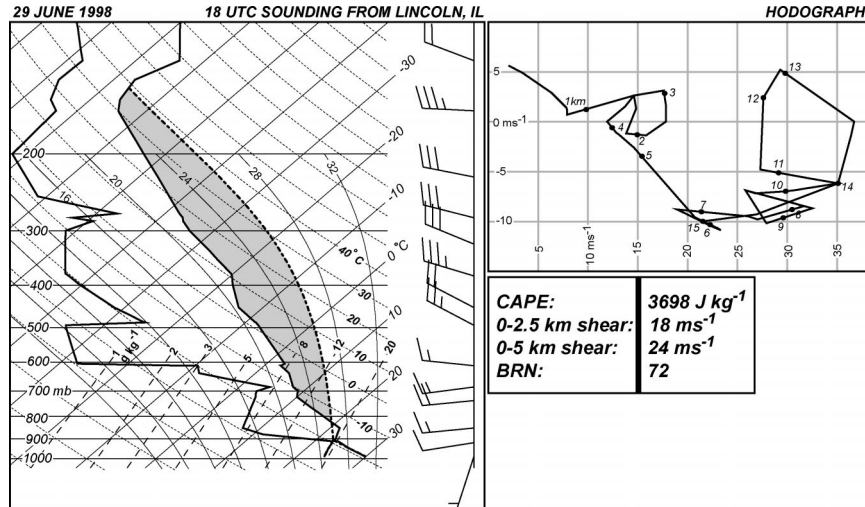
FIG. 2. Sounding and hodograph from Lincoln at 1800 UTC on 29 Jun 1998. The positive area in the sounding is shaded gray. Winds are in meters per second (half barb = 5 m s^{-1}; full barb = 10 m s^{-1}).

served along the stationary front at this time over central Iowa. Supercell thunderstorms were also observed at this time moving quickly eastward from the eastern South Dakota–Nebraska border (not shown). Two hours later at 1815 UTC (Fig. 4b), a linear squall line comprised of discrete supercells is observed over central Iowa (Martinelli et al. 2000) in the region where the outflow boundary has merged with the stationary front. Warm, moist southwesterly flow is observed south of the stationary front and convective system. While not as apparent at 1615 UTC, there appears to be a moisture boundary extending from the midpoint of the squall line southeastward into south-central Illinois with dewpoints in the low 20s north of the boundary and in the low to mid-20s south of the boundary. As the system continues

to move southeastward into the warm sector, the transition to a bow echo structure has occurred by 2015 UTC (Fig. 4c). The stratiform rain region continues to grow in spatial scale behind the leading edge of the convective system, suggesting that the system-scale updrafts have tilted upshear (Rotunno et al. 1988; Weisman 1993). The divergent flow associated with the system's cold pool, or mesohigh (Fujita 1955), is evident at this time. Surface stations at or just behind the leading edge of the bow echo show temperatures nearly 14°C cooler than the ambient values ahead of the system. The moisture boundary observed at 1815 UTC has continued to move northeastward and intersects the bow echo near the apex. An enhanced cumulus field is observed along and to the southwest of the moisture boundary. The bow
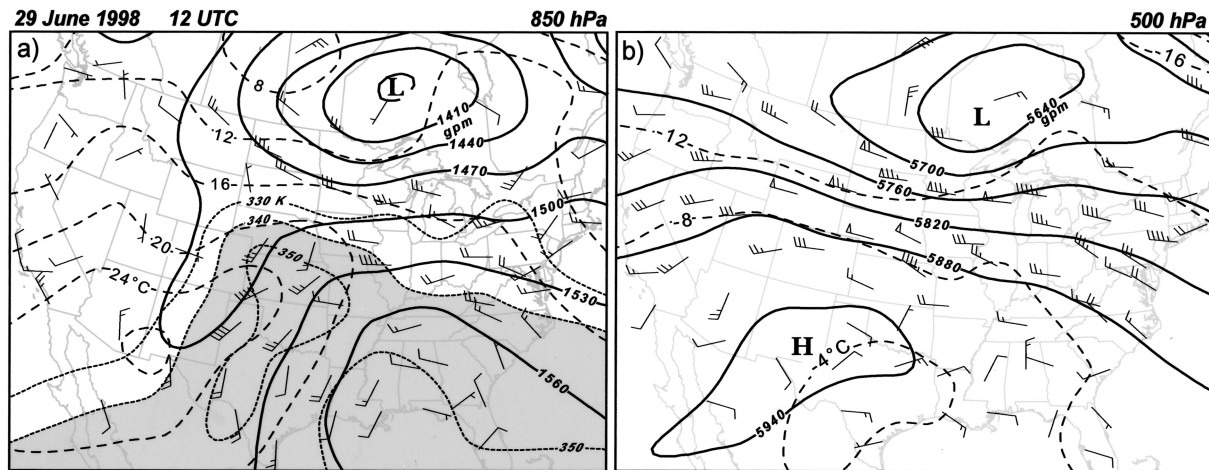

FIG. 3. The 850- and 500-hPa upper-air maps on 29 Jun 1998 at 1200 UTC. Solid and long dashed lines represent geopotential heights (gpm) and temperature (°C), respectively. Winds (half barb = 2.5 m s^{-1}; full barb = 5.0 m s^{-1}; flag = 25 m s^{-1}) are also shown. Equivalent potential temperature (K) is shown in (a) as short-dashed lines, with values greater than 340 K shaded in gray.
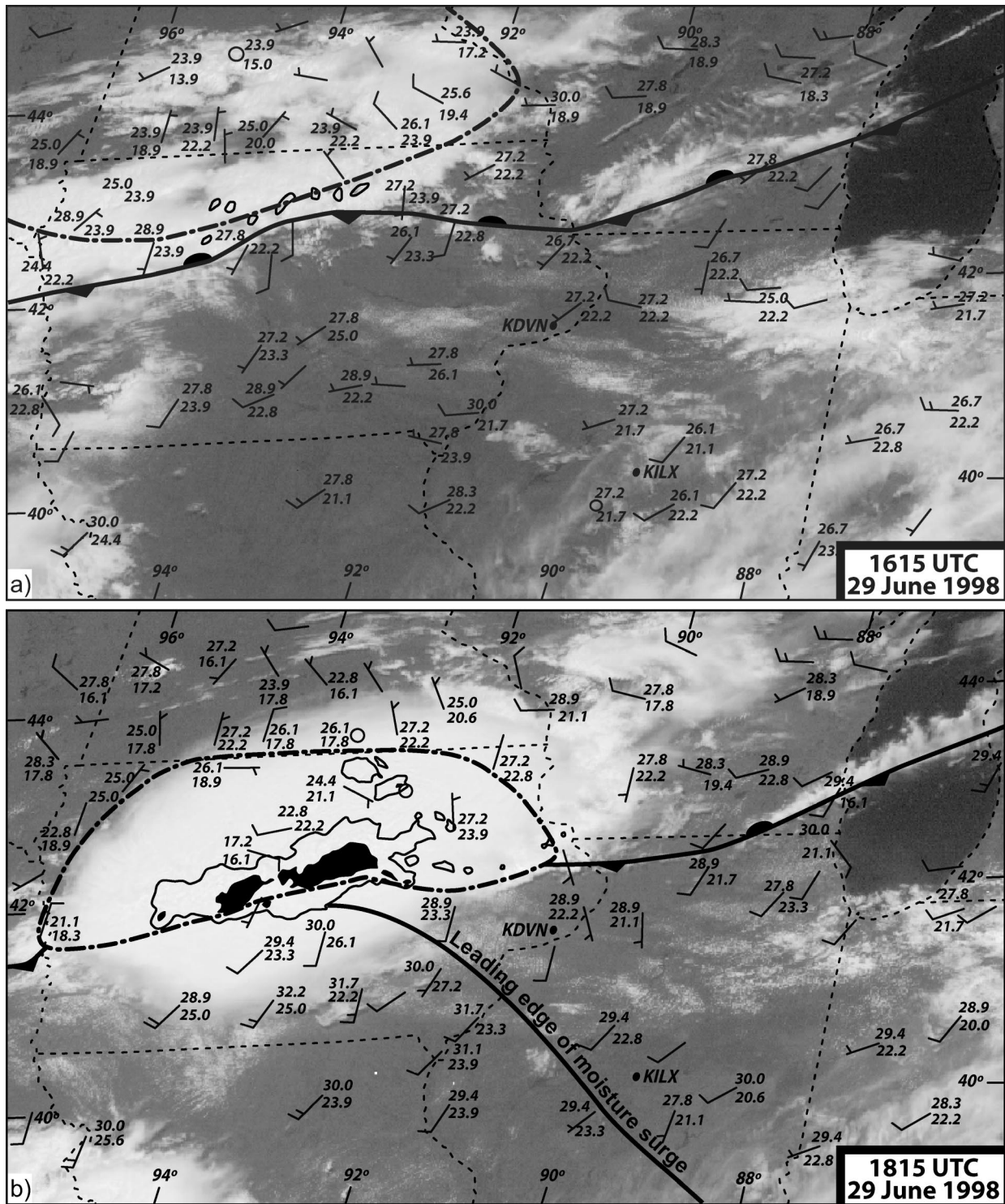
Fig. 4. Satellite analyses at 1615, 1815, 2015, and 2215 UTC on 29 Jun 1998. Superimposed on the visible imagery is surface data showing temperature, dewpoint (both in °C), and winds (same convention used in Fig. 1). Also plotted is the radar reflectivity field (dBZ) from the KDVN and KILX radars, with values equal to 35 and 50 dBZ contoured and shaded in black, respectively. Short-dashed lines are state boundaries. The stationary front, outflow boundary, and leading edge of moisture surge are also indicated.
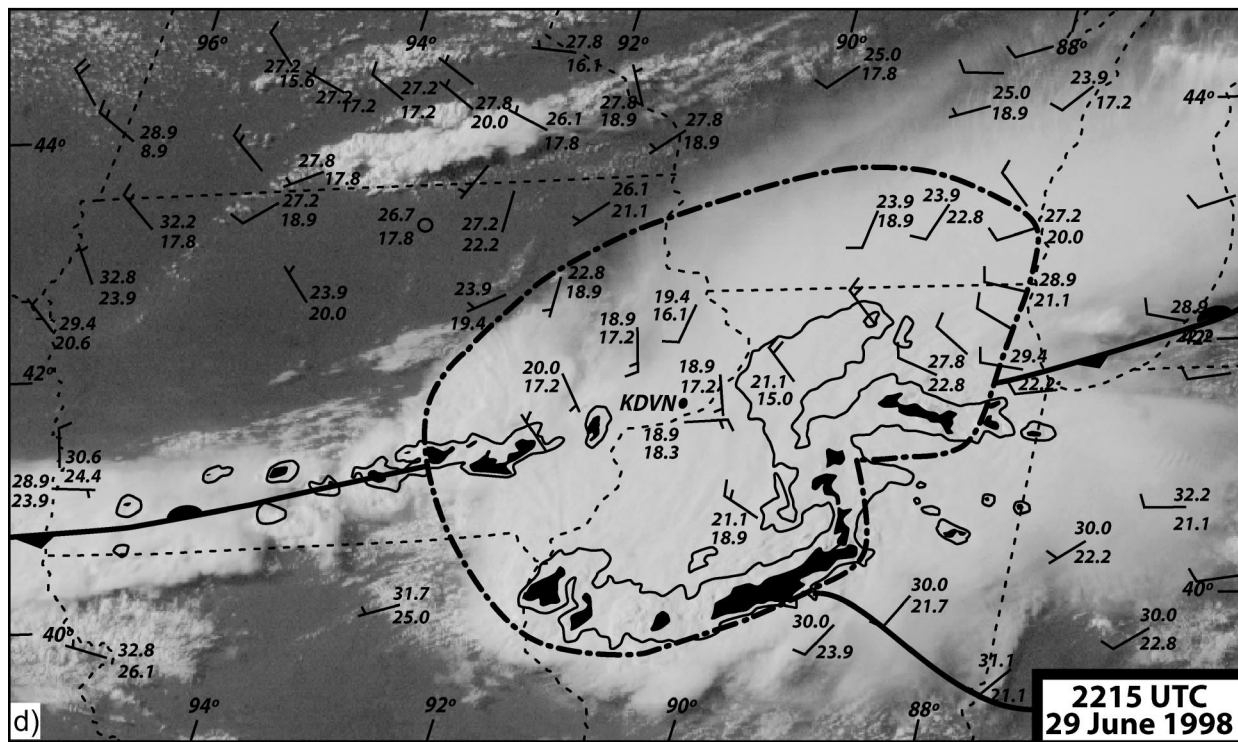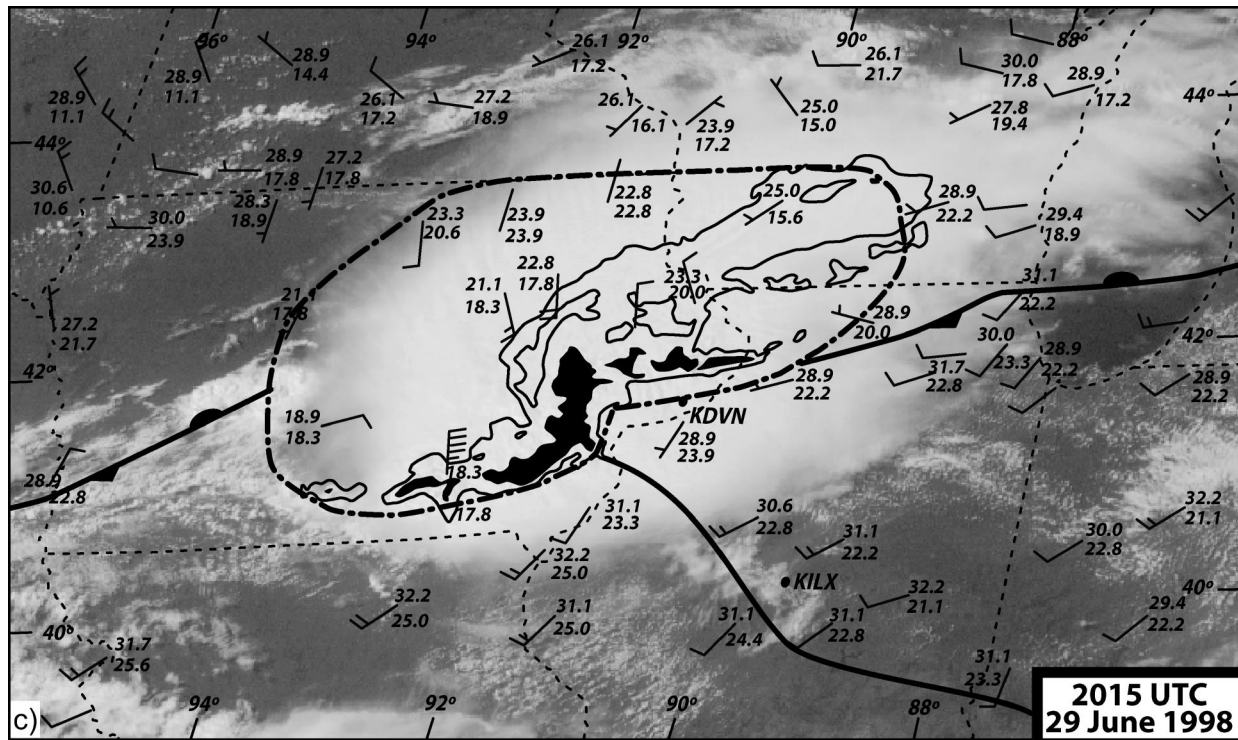
FIG. 4. (*Continued*)

echo continues to move southeastward into central Illinois by 2215 UTC (Fig. 4d) and has grown upscale, with the reflectivity field possessing the "comma shaped" echo structure described by Fujita (1978) or asymmetric squall-line configuration discussed by Houze et al. (1989). The reflectivity field in Fig. 4d suggests a large-scale circulation, or mesoscale convective vortex (MCV), at the northern end of the derecho. Previous observational studies (e.g., Maddox 1983; Bartels and Maddox 1991; Trier et al. 2000) have documented similar midlevel vortices produced by mesoscale convective systems (MCSs). MCVs often persist longer than the parent MCS and have been observed to retrigger convective systems on subsequent days (Johnston 1981; Bartels and Maddox 1991; Menard and Fritsh 1989). Detailed radar observations of this circulation are presented in section 6. Also observed at 2215 UTC are convective cells initiating over southern Iowa along the stationary front, west and north of the primary convective system. These cells eventually evolved into supercell thunderstorms. Divergence with the system's mesohigh is even more prominent at 2215 UTC, suggesting that it has continued to strengthen and deepen with time.

4. Radar depiction of system and subsystem-scale features

During its mature stage, the 29 June 1998 derecho possessed many system and subsystem-scale features that have been previously documented in the literature. Evident in the radar reflectivity field at 2149 UTC (Fig. 5a) is the large bowing segment of convective cells with a noticeable asymmetric stratiform rain region at the northern end of the convective line (Houze et al. 1989). The system has evolved into the comma stage of bow echo evolution (Fujita 1978) with a prominent rotating comma head at the northern end. A tight reflectivity gradient is observed at the leading edge of the system (Przybylinski and Gery 1983; Przybylinski and DeCaire 1985). A distinct rear-inflow notch (RIN) (Przybylinski 1995) is observed in the stratiform rain region behind the leading edge of the system near the bow apex and suggests the presence of a descending mesoscale rear-inflow jet that is entering the convective system from the rear (Smull and Houze 1985, 1987). Owing to the fortuitous view angle from the Lincoln WSR-88D, a 40 m s^{-1} descending rear-inflow jet was, in fact, observed with the system (Figs. 5b,c) collocated with the rear-inflow notch in Fig. 5a. While somewhat subjective, the core of strongest winds associated with the rear-inflow jet appears to be about 60 km in width (Fig. 5c). The vertical cross section in Fig. 5b also shows the ascending front-to-rear flow above the rear-inflow jet (Houze et al. 1989). Also apparent is the multicellular nature of the convective system at this time, where three cells at different stages in their evolution are observed in the reflectivity field in Fig. 5b. This data along with the ob-

served ascending front-to-rear flow suggest that the system-scale cold pool has overwhelmed the ambient shear ahead of the system, tilting the system-scale updrafts upshear (Rotunno et al. 1988; Weisman 1993). Furthermore, the vorticity imbalance appears to be greatest at the bow apex since the convective cells were observed to be taller at the ends of the bow echo than at the apex at 2150 UTC (not shown).

Another obvious system-scale feature evident in the radial velocity data in Fig. 5c is the northern line-end vortex coincident with the comma head echo. The vortex couplet diameter[1] is approximately 20 km at 2151 UTC and is consistent with sizes of bow echo line-end vortices produced in numerical simulations (Weisman 1993). No well-defined anticyclonic line-end vortex is observed on the southern end of the convective system at this time, consistent with numerical simulations by Skamarock et al. (1994) that show how stretching of planetary vorticity with time enhances only the northern line-end vortex.

In addition to the larger-scale line-end vortex, three smaller meso-γ-scale vortices (e.g., Funk et al. 1999; Arnott and Atkins 2002) are observed on the leading edge of the bow echo as enhanced shear regions in the radial velocity field. Two vortices (8 and 9) are located north of the bow apex, while one (6) is found south of the apex. It should be noted that all previous studies documenting the location of vortices formed on the leading edge of bow echoes have placed them at or north of the apex. The observations presented in Fig. 5 and in the next section are believed to be the first to show that meso-γ-scale vortices can form on the leading edge of a bow echo south of the apex.

5. Damage analysis

a. Wind damage

The 29 June 1998 derecho event was a prolific producer of damaging surface winds. Property and crop damage estimates from *Storm Data* (NCDC 1998) were 151 million and 20 million dollars, respectively, for both Iowa and Illinois. Numerous injuries and one fatality resulted from the damaging straight-line winds and tornadoes produced by this derecho.

The time evolution of radar reflectivity for the 29 June 1998 derecho, along with wind damage locations as reported in *Storm Data,* is shown in Fig. 6. Clearly, the most widespread wind damage occurred after the system transitioned into a bow echo at about 1930 UTC. The area of countywide wind damage is centered on the bow echo apex with surface wind damage being reported indiscriminately north and south of the apex location throughout the entire time period shown in Fig. 6. The

---

[1] All vortex diameters reported in this paper refer to the radial velocity couplet diameter. It is recognized that the actual circulation diameter will be larger.
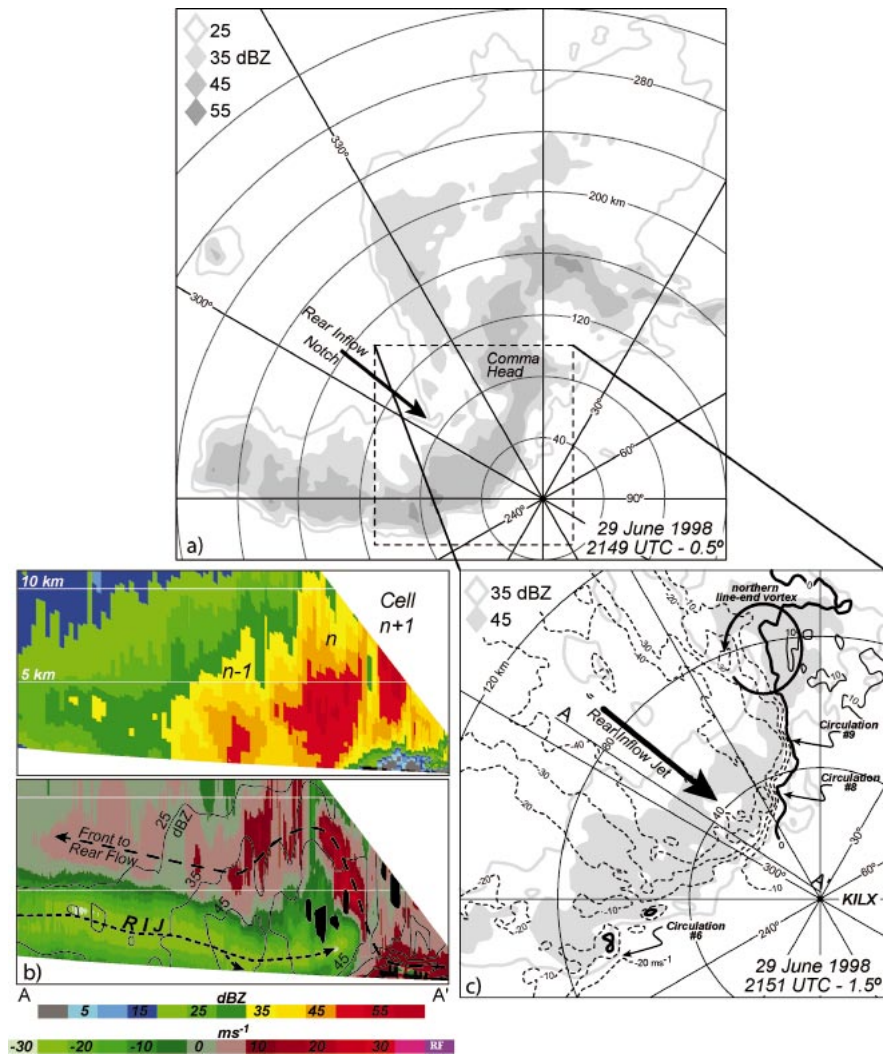
FIG. 5. (a) Radar reflectivity at 2149 UTC from the KILX 0.5° elevation angle scan. (b) Vertical cross section through the RIJ along the path labeled A–A′ in (c). Shown are the radar reflectivity and storm-relative radial velocities [cool (warm) colors indicate velocities toward (away) from the radar]. Black contours of reflectivity are superimposed on the velocity image. (c) Radar reflectivity (gray) and ground relative radial velocities are shown with solid (away) and dashed (toward) black lines.

spatial extent of the wind damage reports increases with time, consistent with the observation that the convective system is also observed to increase in size as it propagated southeastward.

b. Tornado damage

Similar to the derecho event discussed by Funk et al. (1999), the 29 June 1998 derecho produced many small-scale circulations formed at the leading edge of the convective system. These circulations were detected in the Davenport and Lincoln WSR-88D radial velocity data. Their locations are shown in Fig. 7 along with tornadic report locations from *Storm Data.* A total of 13 circulations were observed. Striking in Fig. 7 is the close

association between *Storm Data* tornado reports[2] and radar-detected circulation locations. This close association lends credence to the *Storm Data* tornado reports for this case and helps to discriminate between the tornadic and nontornadic vortices, as 7 of the 13 vortex tracks are collocated with tornado reports of F0–F1 intensity. Forbes and Wakimoto (1983) have previously shown that bow echoes can be prolific producers of tornadic damage. Also apparent is that the vortices and tornado damage first appeared shortly after the system began its transition to a bow echo. Many of the vortices

[2] A detailed damage survey of this event was performed by National Weather Service personnel from both the Davenport and Lincoln offices, including the fourth author of this paper.
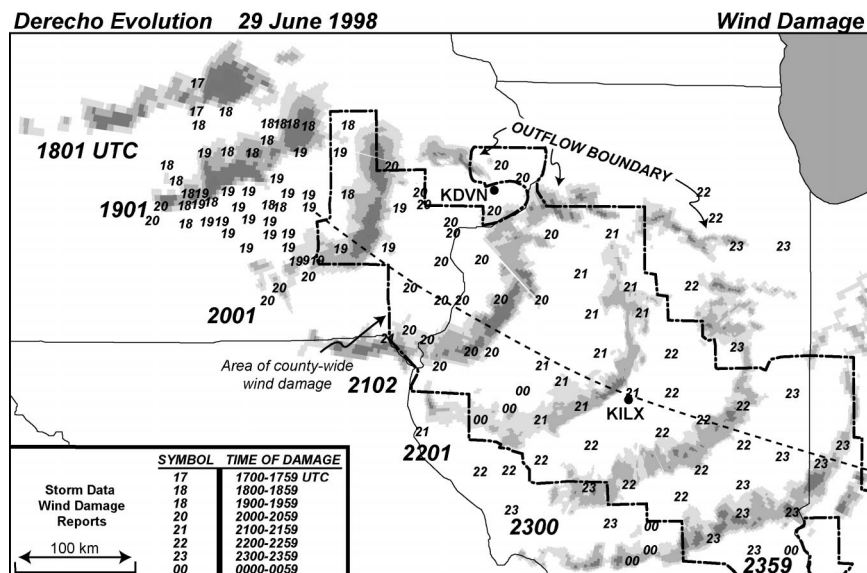
FIG. 6. Radar reflectivity (dBZ) at 1801, 1901, 2001, 2102, 2201, 2300, and 2359 UTC on 29 Jun 1998 is shown in gray along with locations of wind damage reports from *Storm Data.* The dashed–dotted line represents the area encompassing countywide wind damage reports. The long-dashed line represents the location of the primary bow echo apex.

moved in a direction parallel to the bow apex while others appeared to move northward relative to the apex location. This observation is somewhat different than the results of Weisman and Trapp (2003) who showed that all simulated mesovortices moved northward relative to the bow apex location. Striking in Fig. 7 is that not all of the vortices are formed north of the bow echo apex. In fact, three of the vortices are observed south of the apex, and one of them (11) was tornadic. All three of these circulations south of the apex were cyclonic and not associated with midlevel rotation, similar to those vortices north of the apex. These observations are contrary to previous studies that have documented tornadic and nontornadic vortices to form only at or north of the bow echo apex (e.g., Funk et al. 1999).

6. Vortex characteristics

a. Mesovortices

Owing to the close proximity of the KDVN and KILX WSR-88Ds to the convective line and advantageous view angles, circulations on the leading edge of the derecho were readily detected in the single-Doppler velocity data. An example at 2019 UTC is shown in Fig. 8, in which reflectivity and storm-relative radial velocity data from KDVN are shown for the lowest four elevation angles. Three of the mesovortices (1, 3, and 5) shown in Fig. 7 are observed in the 0.5° data in Fig. 8a. All three circulations are visible as a rotational velocity couplet or enhanced shear signature. Unlike the other mesovortices, vortex 1 forms just south of the intersection point of the primary convective line and the east–west outflow boundary shown in Fig. 4. Previous

investigators (e.g., Schmocker et al. 2000; Przybylinski et al. 2000; Wolf 2002) have shown that the intersection location between the primary convective line and an east–west-oriented boundary is a preferred region for mesovortex genesis. Another unique feature of vortex 1 is that it has a spatial scale that is much larger than all other mesovortices formed within the 29 June 1998 derecho. The reason for this size difference is not well understood but may suggest that the genesis mechanism for vortex 1 is different than for the other mesovortices. All three mesovortices are evident at all other elevation angles shown in Fig. 8 and are located on the reflectivity gradient, suggesting that they have formed on the cool-air side of the gust front. Another boundary is also evident, particularly in the reflectivity field, intersecting the bow echo at or just north of the apex. It is possible that this boundary is connected to the moisture surge evident in the surface analysis on the satellite imagery presented in Fig. 4. It is interesting that vortex 3 forms near the intersection of this boundary and the primary convective line, suggesting that the interaction between them may play a role in the genesis of vortex 3.

In addition to the leading-edge vortices, an embedded pair of bookend vortices is observed only in the 2.4° and 3.3° elevation slices north of the primary bow apex and behind the leading edge of the system updrafts. While numerical simulations (Weisman and Davis 1998) have generated embedded bow echoes such as the one shown in Figs. 8c and 8d, observations corroborating their existence are not well documented in the literature. Detailed analyses of this embedded bow echo and another that formed at a later time are shown in section 6b.
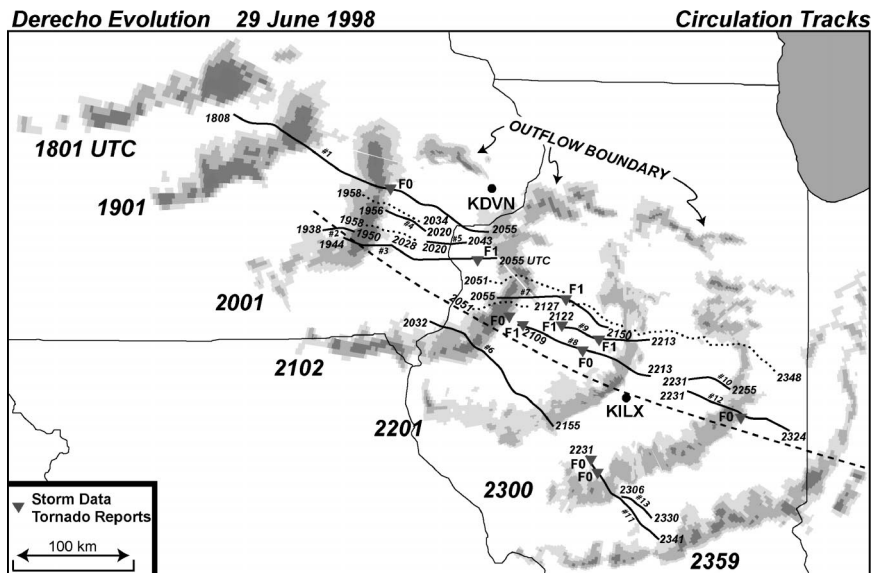
FIG. 7. As in Fig. 6, radar reflectivity is shown in gray. Solid black lines with start and end times represent the tracks of radar-detected circulations. The short-dashed lines represent the locations of radar-detected bookend vortices. The long-dashed line indicates the location of the primary bow echo apex. Tornado report locations and intensity from *Storm Data* are indicated with gray triangles.

1) MESOVORTEX SIZES

Consistent with previous observational studies, the 29 June 1998 mesovortices had couplet diameters that ranged from about 0.5 to 9 km as shown in Fig. 9. Note that a few of the vortices have initial sizes less than 2 km, suggesting that early detection of these vortices at long ranges can be problematic. The anomalously large size of vortex 1 is again evident.

Recent numerical simulations by Weisman and Trapp (2003) have shown simulated mesovortices to decrease in number and grow upscale with time. Eventually, some of the mesovortices grow in size comparable to and even evolve into the bookend vortices. The observations in Figs. 7 and 9, however, do not corroborate this simulation result. The number of vortices forming on the leading edge of the 29 June 1998 derecho does not diminish with time (Fig. 7), and the vortex core diameters show no consistent trends in Fig. 9. While some of the vortices do become larger with time, their resultant size is still much smaller than observed and simulated sizes for bookend vortices.

2) VORTEX LIFETIMES

An interesting aspect of mesovortex evolution within the 29 June 1998 derecho is that all vortices, with the exception of 1, formed after the system evolved into a bow echo (Fig. 10). Multiple vortices were observed concurrently at various points in their lifetimes, similar to the results of Funk et al. (1999). The vortices appear to form continuously during the entire lifetime of the bow echo. The mean vortex lifetime is relatively short,

only 56 min compared to an average lifetime of about 90 min for the midlevel mesocyclone observed within supercell thunderstorms (Burgess et al. 1982). A striking observation in Fig. 10 is that the nontornadic vortices are consistently shorter lived than their tornadic counterparts. The average lifetimes for the nontornadic and tornadic vortices are 32 and 76 min, respectively. When excluding mesovortex 1, mean tornadic lifetime is still 61 min. The reason why the tornadic vortices within the 29 June 1998 derecho persist longer is not well understood. This issue will be further explored in Part II.

3) MESOVORTEX STRENGTH

In addition to vortex lifetime, another interesting difference observed between the tornadic and nontornadic mesovortices is that the tornadic vortices consistently have stronger rotational velocities. This is shown in Fig. 11, in which time–height profiles of V_r (see Fig. 11d for definition) are plotted for two representative nontornadic (Figs. 11a,b) and tornadic (Figs. 11c,d) vortices. Note that for all four vortices, there is no midlevel rotation that precedes low-level rotation, suggesting that the mesovortices are ''nondescending'' (Trapp et al. 1999) in nature. In all cases, the strongest V_r values are found at low levels. Clearly, however, the tornadic vortices are associated with larger V_r values, suggesting that they have larger rotational velocities than the nontornadic vortices. The nontornadic vortices generally have V_r values less than 20 m s^{-1}, while the tornadic vortices often have values greater than 25 m s^{-1}.

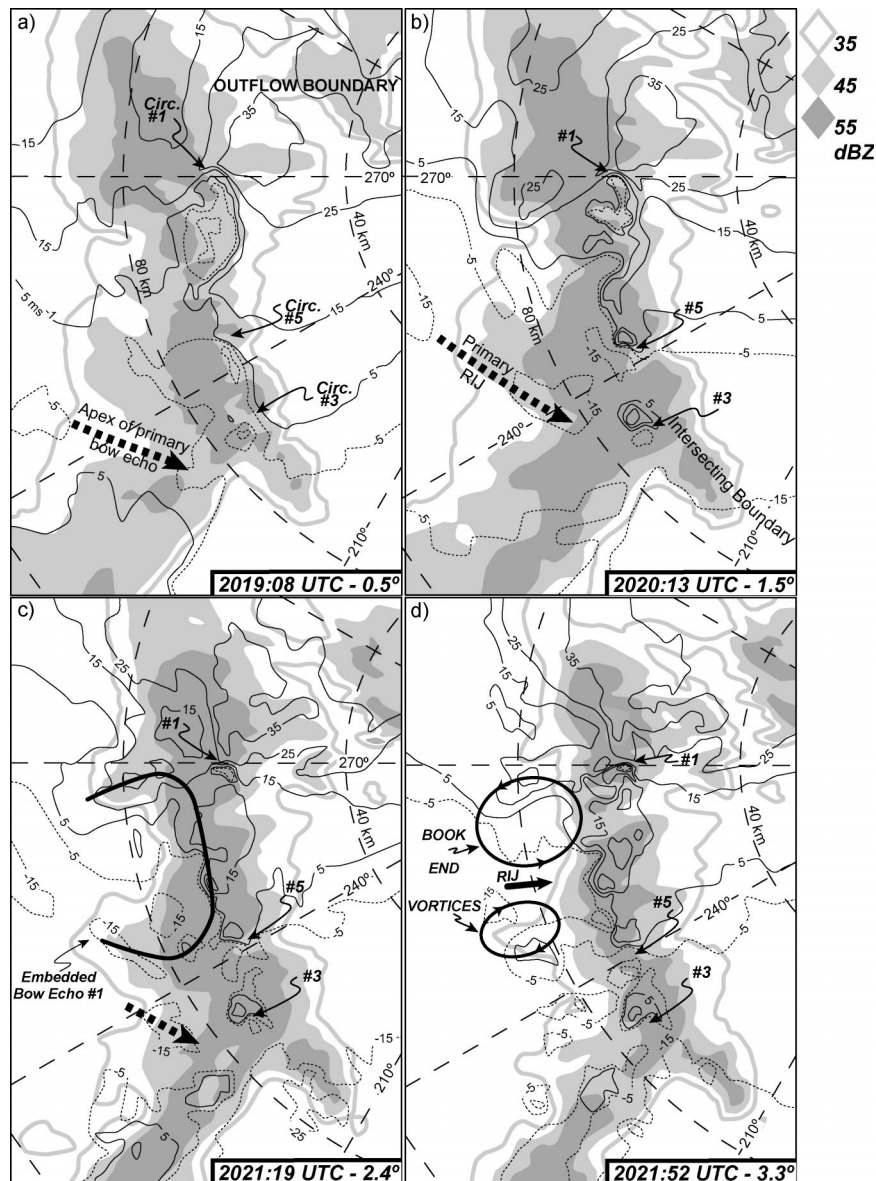The differences in vortex strength are even more ap-

FIG. 8. Radar reflectivity and storm-relative radial velocities from 2019:08 to 2021:52 UTC. Elevation angles of 0.5°, 1.5°, 2.4°, and 3.3° are shown. Solid and dashed radial velocities indicate flow away and toward the radar, respectively. Thin dashed black lines are range rings and azimuths relative to the KDVN radar. The thick black line in (c) delineates the location of embedded bow echo 1.

parent when looking at mean V_r vertical profiles for all tornadic and nontornadic vortices, as shown in Fig. 12. A striking observation in Fig. 12 is that the difference in strength between the tornadic and nontornadic vortices is apparent below 2 km, with the greatest difference of about 8 m s^{-1} below 0.5 km. The results in Figs. 10–12 suggest that it may be possible to distinguish between tornadic and nontornadic vortices within bow echoes as the tornadic vortices tend to be stronger and longer-lived. However, as shown in Fig. 12, the strength difference is greatest below 2 km. Thus, accurate mon-

itoring of the time history of low-level vortex strength and longevity may be useful in the warning process for distinguishing between tornadic and nontornadic vortices formed within quasi-linear convective systems.

b. Bookend vortices

Numerical simulations have shown that the bookend vortices are a fundamental system-scale feature of bow echoes that can enhance the rear-inflow jet (RIJ) by 30%–50% (Weisman 1993) and may have a role in tor-
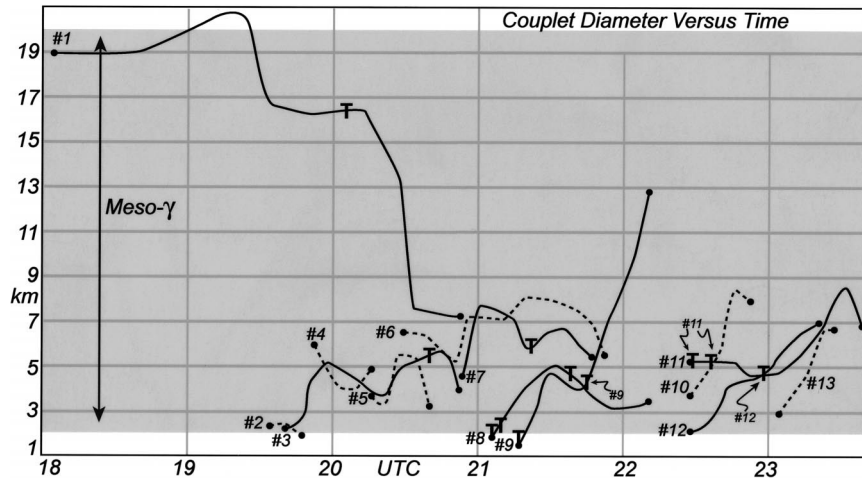
FIG. 9. Time series of couplet diameter for all of the mesovortices whose positions are shown in Fig. 7. The ''T''s indicate time of tornado occurrence for the associated vortex. Dashed lines indicate nontornadic vortices.

nadogenesis (Pfost and Gerard 1997). Weisman and Davis (1998) have further shown with idealized simulations that smaller-scale embedded bow echoes and bookend vortices can be produced within a larger-scale bow echo. Detailed radar observations of bookend vortices on any scale, however, are not well documented in the literature. Fortunately, both the KDVN and KILX WSR-88Ds were able to observe the evolution of two sets of bookend vortices associated with two embedded bow echoes.

The first embedded bow echo formed approximately 20 min after the primary convective system began to bow outward (Fig. 7) and persisted for about 36 min. Radar observations of this bow echo are shown in Figs. 8c and 8d. Note that it is located north of the primary

bow apex and has a small spatial scale of about 30 km. The bookend vortices are observed in the 2.4° and 3.3° elevation scans (Figs. 8c,d) and appear to be responsible for advecting precipitation rearward of the leading edge. A smaller-scale RIJ is observed between the bookend vortices and is not associated with the larger convective system RIJ.

The evolution of vortex depth and size is shown in the time–height diagram of velocity couplet diameter in Fig. 13. Clearly, both bookend vortices are observed at midlevels between 3 and 9 km. The northern bookend vortex is initially larger than 20 km in diameter and evolves to a size less than 15 km at the latter stages of its evolution. The southern anticyclonic bookend vortex diameter is consistently about 12–13 km.
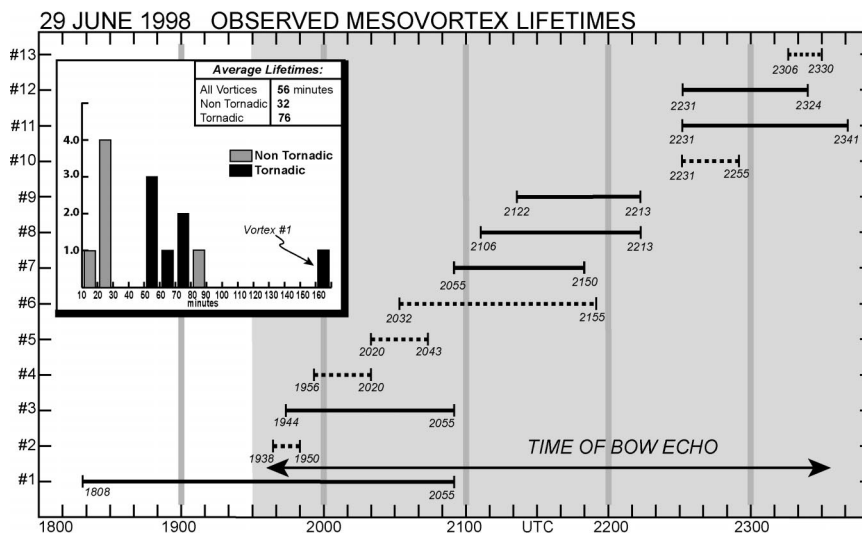

FIG. 10. Lifetimes of all leading edge vortices shown in Fig. 7. Vortex number is indicated on the vertical axis. The primary bow echo was observed during the time period shown in gray. Dashed lines indicate nontornadic vortices. The inset diagram is a histogram of vortex lifetimes.
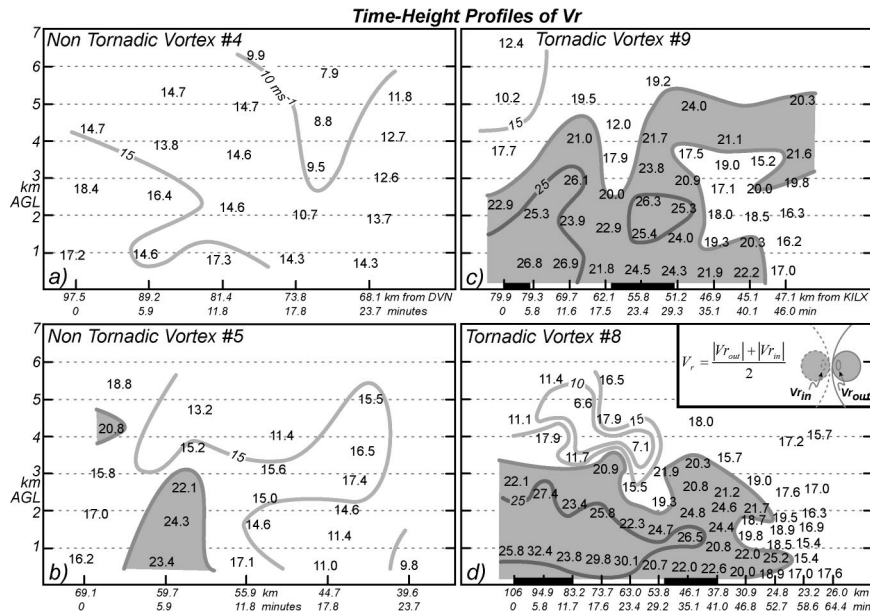
FIG. 11. Time–height profiles of average radial velocity, V_r for nontornadic vortices 4 and 5 and tornadic vortices 9 and 8. As shown in the inset diagram, V_r is defined as the average of the absolute values of the inbound and outbound radial velocity values associated with the rotational couplet; V_r values are contoured every 5 m s^{-1}, with values greater than 20 m s^{-1} shaded gray. The black bars in (c) and (d) represent the time periods of tornadic damage.

Approximately 15 min later at 2051 UTC, another embedded bow echo and bookend vortex pair form north of the primary bow echo apex (Fig. 7). As shown in Fig. 14b, the southern anticyclonic vortex persists for about 30 min, is observed between 4 and 13 km and

FIG. 12. Composite vertical profiles of V_r for all tornadic (solid line) and nontornadic (dashed line) mesovortices shown in Fig. 7. Error bars represent 1 std dev for all data points at the respective level.

has a diameter of roughly 10 km. These observations are similar to those of the anticyclonic vortex associated with the first embedded bow echo. The evolution of the northern cyclonic bookend vortex, however, is much different than what was observed with the first embedded bow echo. This vortex is first observed between 3 and 9 km with a diameter of about 20 km (Fig. 14a). Shortly after the time of genesis, the vortex appears to decrease in size until approximately 2125 UTC when it then continuously grows in scale. The vortex is also observed to descend with time beginning at approximately 2114 UTC and is subsequently observed below 1 km AGL by 2155 UTC. There appears to be a strong correlation between the northern bookend vortex lowering to the ground and the strength of the observed surface winds and amount (in dollars) of damage as reported in *Storm Data* that can be associated with the vortex. Figure 14a clearly shows that the strongest wind gusts and greatest amount of damage occurred when the vortex was observed closest to the ground over Tazewell County, Illinois. Idealized numerical simulations (Trapp and Weisman 2003) have also shown that the strongest near-surface winds may be associated with such vortices. The results in Fig. 14a suggest that monitoring bookend vortex location and its vertical extent may be useful for identifying areas prone to high surface winds. Thereafter, the vortex is observed only at midlevels and continues to grow in size, greater than 40 km, after 2300 UTC. Thus, unlike the first cyclonic embedded bookend vortex, the second is longer-lived, deeper, and much larger. In fact, the second cyclonic bookend vortex be-
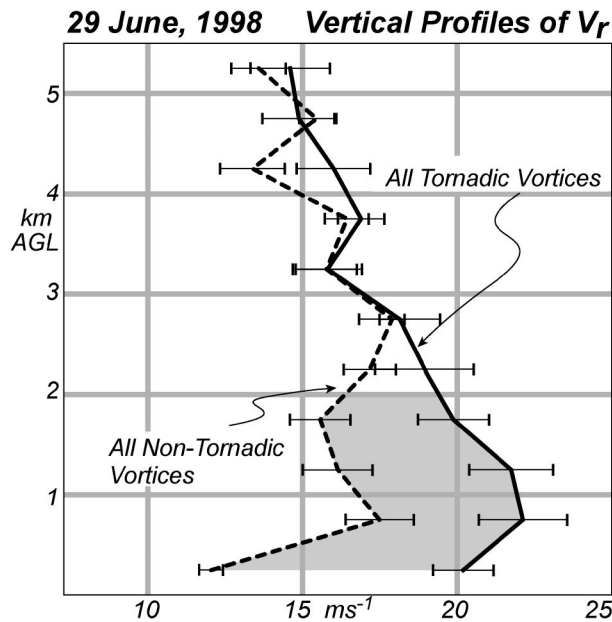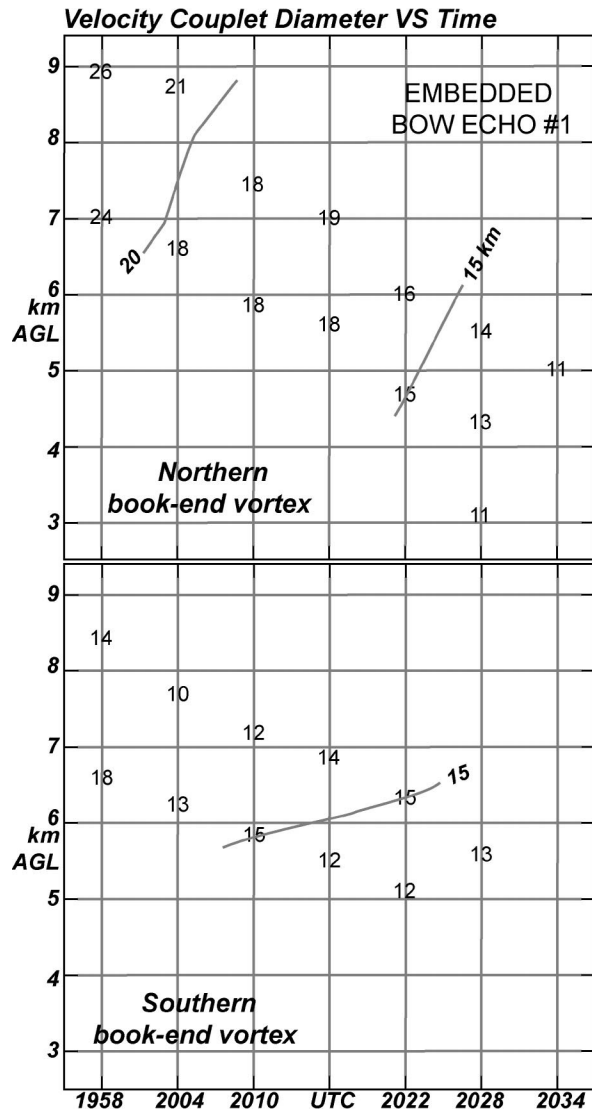
FIG. 13. Radial velocity couplet diameter (km) vs time for the northern and southern bookend vortices associated with embedded bow echo 1 shown in Fig. 8.

collocated curling reflectivity pattern are better defined. During the next 40 min (Figs. 15c,d) the vortex appears to move northward and rearward relative to the primary bow apex and is now located at the northern end of the convective system, becoming the primary system's northern line-end vortex. Northward vortex motion relative to apex location has been documented in numerical simulations (Trapp and Weisman 2003). Upscale growth is also observed in this time period. The velocity couplet becomes ill defined at 2215 and 2233 UTC owing to its position relative to the radar viewing angle. The circulation can be inferred, however, in the reflectivity field, especially at 2233 UTC where the existence of a weak echo hole is centered on the couplet location. Weak echo holes are commonly observed with strong circulations (e.g., Wakimoto and Martner 1992; Wurman and Gill 2000). The vortex continues to grow in size and is located further rearward of the leading edge of the convective system and north of the well-developed RIJ (Fig. 15e). By 2256 and 2314 UTC (Figs. 15g,h) the couplet is again better defined. The circulation is apparent in the reflectivity field, especially at 2256 UTC where a curling pattern is visible in the stratiform rain region behind and north of the primary convective line.

After the cyclonic vortex migrated to the northern end of the convective line, its evolution is very similar to the numerical simulations by Weisman and Davis (1998), who showed that the line-end vortices would tend to move rearward relative to the leading edge of the convective system later in its evolution and grow in size. The vortices would move further rearward when the environmental shear at low levels was weaker. The rearward propagation is a result of the system-scale updraft tilting upshear as the strengthening cold pool begins to overwhelm the environmental shear. As discussed in section 3, the cold pool associated with the 29 June 1998 derecho was in fact quite strong during its mature stage. Evidence that the system-scale updraft had already tilted upshear by 2151 UTC is seen in Fig. 5.

7. Discussion and summary

In Part I of this two-part paper, radar and damage observations of the progressive derecho event formed on 29 June 1998 over Iowa and Illinois have been presented. More specifically, the structural evolution of low and midlevel vortices formed along and behind the leading edge of the convective system, respectively, have been shown.

A total of 13 low-level mesovortices were observed within the derecho with all but 1 of them forming after the system evolved into a bow echo. Only 10 of the mesovortices formed north of the bow apex; the remaining 3 formed south of the apex. Combining *Storm Data* tornado reports with the radar data showed that seven of the mesovortices were tornadic. Tornadic mesovortices were observed both north and south of the bow apex. Mesovortex diameters were small in scale,

comes the system's dominant line-end vortex. This can best be seen in the time series observations of radar reflectivity and Doppler radial velocities in Fig. 15. Five minutes after the vortex was initially detected at 2051 UTC (Fig. 15a), the vortex is readily apparent as a radial velocity couplet collocated with a curling pattern in the radar reflectivity field. The couplet diameter at this time is about 20 km. It is important to note that the vortex is not located on the northern end of the primary convective system as the convective line is observed to extend well north of the vortex location, confirming that it is associated with an embedded bow echo. The intersecting boundary shown in Fig. 8 is also apparent in the reflectivity data in Fig. 15a between approximately 60 and 100 km at an azimuth of 165°. Twenty minutes later at 2115 UTC (Fig. 15b), the velocity couplet and
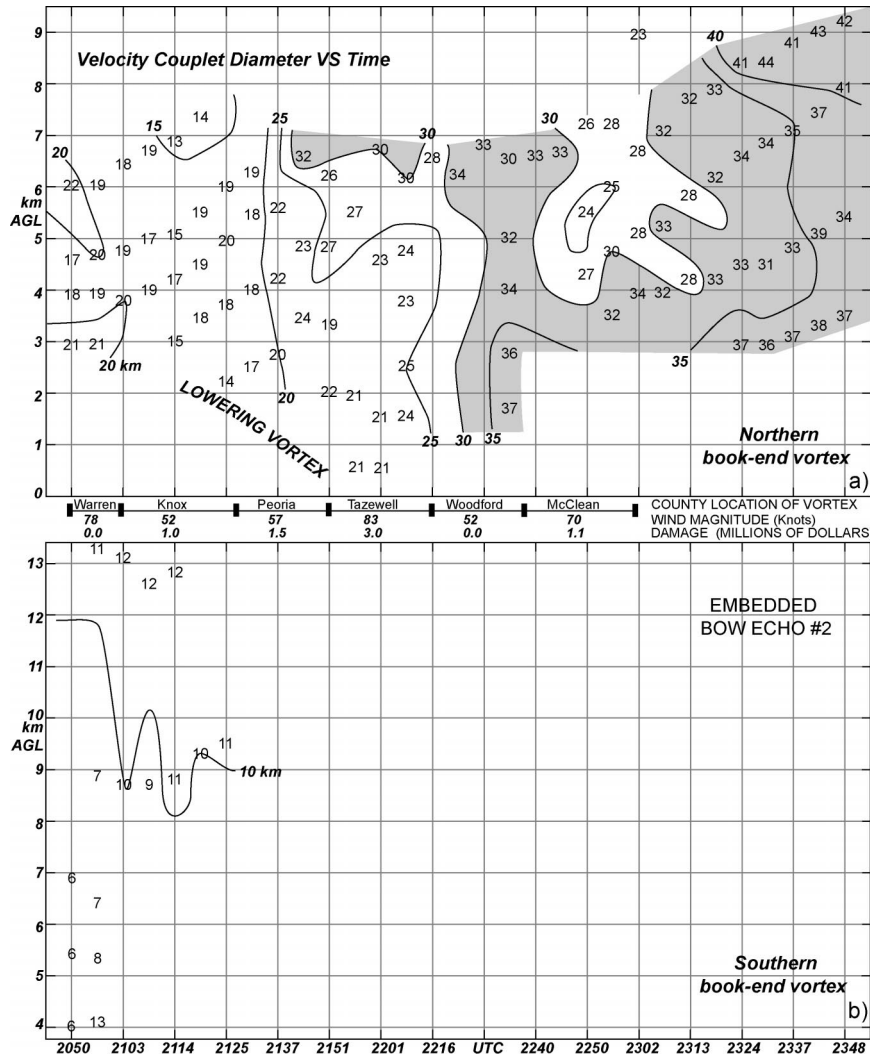
FIG. 14. Radial velocity couplet diameter (km) vs time for (top) the northern and (bottom) southern bookend vortices associated with embedded bow echo 2. Values greater than 30 km are shaded gray.

generally ranging from 0.5 to 9 km. Appreciable upscale growth was not observed with any of the mesovortices.

Close examination of the radar data suggests that it may be possible to distinguish between the tornadic and nontornadic mesovortices. Consistently, the tornadic mesovortices exhibited larger rotational velocities. Tornadic mesovortices often exhibited V_r magnitudes in excess of 25 m s^{-1} while the nontornadic vortices often were characterized by V_r magnitudes less than 20 m s^{-1}. The difference in mesovortex strength was largest below 2 km AGL with the greatest difference of about 8 m s^{-1} near ground level.

Another robust observation concerns vortex longevity. Mean mesovortex lifetime was about 56 min. Mean lifetimes for the tornadic and nontornadic mesovortices were 76 and 32 min, respectively. Thus, by monitoring the temporal evolution of mesovortex strength and lon-

gevity, forecasters may be able to discern between tornadic and nontornadic vortices formed within QLCSs. Further observational studies are needed to test the generality of these results.

It is interesting to compare the detection problem of tornadic circulations within supercell thunderstorms to those observed within QLCSs. Supercell thunderstorms are characterized by persistent midlevel rotation with typical diameters of 7–10 km. Thus, with respect to vortex size, supercell mesocyclones are more likely to be detected than QLCS mesovortices, especially at longer ranges.

Studies by Burgess et al. (1993) and Trapp and Stumpf (2002) have shown, however, that only a small fraction (less than 30%) of supercells produce tornadoes. It is well established that many tornadoes form within a separate low-level mesocyclone. Interestingly,
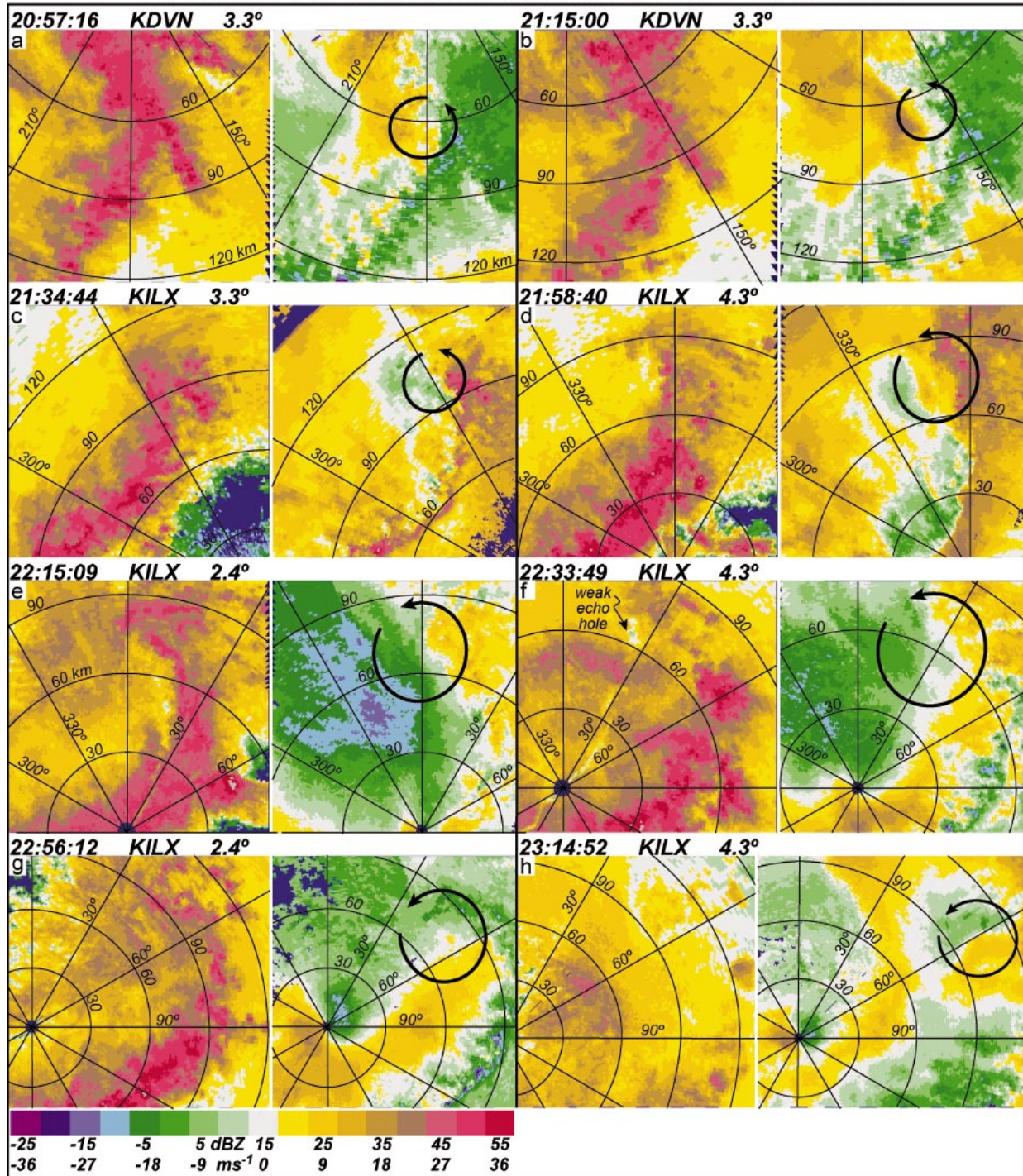
FIG. 15. Time series of radar reflectivity (dBZ) and storm-relative radial velocity (m s^{-1}) for the dominant northern line-end vortex whose position is indicated in Fig. 7. The black circular arrow represents the approximate location of the vortex couplet.

high-resolution Doppler radar observations from the Verification of the Origins of Rotation in Tornadoes Experiment (VORTEX) have shown that the presence of a strong, persistent low-level mesocyclone is not a sufficient condition for tornadogenesis. Both Wakimoto and Cai (2000) and Trapp (1999) have shown that it is not possible to discriminate between tornadic and nontornadic low-level mesocyclones within supercell thun-

derstorms. Hence, while the rotational feature within supercells may be easier to detect with Doppler radar owing to their larger size when compared to QLCS mesovortices, our current understanding does not allow for discrimination between tornadic and nontornadic supercell mesocyclones. On the other hand, the results of this paper suggest that it may be possible to discriminate between tornadic and nontornadic QLCS mesovortices even though they may be harder to detect owing to their smaller size.

Finally, radar observations of midlevel bookend vortices were presented in association with two embedded bow echoes. The first pair of bookend vortices formed approximately 20 min after the primary convective system transitioned into a bow echo and were located north of the apex. They had a lifetime of about 30 min, were observed between 3 and 9 km AGL, and had diameters of 10–26 km. A second embedded bow echo formed approximately 20 min after the first, again north of the primary convective system apex. While the anticyclonic member of this pair persisted for approximately 35 min, the cyclonic vortex persisted for at least 2 h, grew in depth and size, and eventually became the dominant northern line-end vortex of the derecho. The cyclonic vortex descended to near ground level for approximately 10 min and appeared to be responsible for creating enhanced surface wind damage.

While observations of the 29 June 1998 derecho have provided additional insight on vortex structure and evolution within such events, many unresolved issues remain that are critical to the detection and warning process. First, it is not well known when in the life cycle of the QLCS mesovortices tend to form. The results presented herein suggest that they have a tendency to form after the system has transitioned into a bow echo; however, the generality of this observation is not known. This behavior is consistent with idealized bow echo simulations (Weisman and Davis 1998; Weisman and Trapp 2003; Trapp and Weisman 2003). Another important unresolved question is how much lead time is there from initial vortex genesis to the time of tornadogenesis. Furthermore, it is not known why some mesovortices become tornadic and others do not. In an attempt to resolve these questions, future research should, in part, focus on integrating high-resolution radar observations of the mesovortices with detailed damage surveys (e.g., Fujita 1981) rather than *Storm Data* damage reports.

Finally, the mechanism(s) that produces the mesovortices is not well understood. Previous investigators have speculated that the initial vertical vorticity is generated through a release of a horizontal shearing instability (e.g., Forbes and Wakimoto 1983; Przybylinski 1995), tilting of horizontal baroclinic vorticity at the intersection point of a preexisting boundary (e.g., Przybylinski et al. 2000), or tilting of crosswise vorticity by convective-scale downdrafts (Trapp and Weisman 2003). In Part II of this paper, numerical simulations of the 29 June 1998 derecho event with the WRF model will be presented. Preliminary results have already been reported by Atkins and Arnott (2002). The model initialization is a horizontally homogeneous representation of the 29 June 1998 environment using an 1800 UTC Lincoln, Illinois, sounding. Vorticity diagnostics will be utilized to understand the generation mechanism(s) and evolution of mesovortices formed within the simulated convective system. Understanding the mesovortex genesis mechanism(s) will ultimately lead to improved warnings of severe weather produced within QLCSs.

REFERENCES

Arnott, J. M., and N. T. Atkins, 2002: Tornadogenesis within quasi-linear convective systems. Part I: Radar and storm damage analysis of the 29 June 1998 derecho. Preprints, *21st Conf. on Severe Local Storms,* San Antonio, TX, Amer. Meteor. Soc., 494–497.

Atkins, N. T., and J. M. Arnott, 2002: Tornadogenesis within quasi-linear convective systems. Part II: Preliminary WRF simulation results of the 29 June 1998 derecho. Preprints, *21st Conf. on Severe Local Storms,* San Antonio, TX, Amer. Meteor. Soc., 498–501.

Bartels, D. L., and R. A. Maddox, 1991: Midlevel cyclonic vortices generated by mesoscale convective systems. *Mon. Wea. Rev.,* **119,** 104–118.

Bentley, M. L., and T. L. Mote, 1998: A climatology of derecho producing mesoscale convective systems in the central eastern United States, 1986–95. Part I: Temporal and spatial distribution. *Bull. Amer. Meteor. Soc.,* **79,** 2527–2540.

Burgess, D. W., and B. F. Smull, 1990: Doppler radar observations of a bow echo associated with a long-track severe windstorm. Preprints, *16th Conf. on Severe Local Storms,* Kananaskis Park, AB, Canada, Amer. Meteor. Soc., 203–208.

——, V. T. Wood, and R. A. Brown, 1982: Mesocyclone evolution statistics. Preprints, *12th Conf. on Severe Local Storms,* San Antonio, TX, Amer. Meteor. Soc., 422–424.

——, R. J. Donaldson Jr., and P. R. Desrochers, 1993: Tornado detection and warning by radar. *The Tornado: Its Structure, Dynamics, Prediction and Hazards, Geophys. Monogr.,* No. 79, Amer. Geophys. Union, 203–221.

DeWald, V. L., and T. W. Funk, 2000: WSR-88D reflectivity and velocity trends of a damaging squall line event on 20 April 1996 over south-central Indiana and central Kentucky. Preprints, *20th Conf. on Severe Local Storms,* Orlando, FL, Amer. Meteor. Soc., 177–180.

——, ——, J. D. Kirkpatrick, and Y.-J. Lin, 1998: The 18 May 1995 squall line over south-central Kentucky: An examination of complex storm reflectivity trends and multiple mesocyclone development. Preprints, *16th Conf. on Weather Analysis and Forecasting,* Phoenix, AZ, Amer. Meteor. Soc., 148–151.

Evans, J. S., and C. A. Doswell, 2001: Examination of derecho environments using proximity soundings. *Wea. Forecasting,* **16,** 329–342.

Forbes, G. S., and R. M. Wakimoto, 1983: A concentrated outbreak of tornadoes, downbursts and microbursts, and implications regarding vortex classification. *Mon. Wea. Rev.,* **111,** 220–236.

Fujita, T. T., 1955: Results of detailed synoptic studies of squall lines. *Tellus,* **7,** 405–436.

——, 1978: Manual of downburst identification for project Nimrod. Satellite and Mesometeorology Research Paper 156, Dept. of Geophysical Sciences, University of Chicago, 104 pp.

——, 1981: Tornadoes and downbursts in the context of generalized planetary scales. *J. Atmos. Sci.,* **38,** 1511–1534.

——, and H. R. Byers, 1977: Spearhead echo and downburst in the crash of an airliner. *Mon. Wea. Rev.,* **105,** 129–146.

Funk, T. W., K. E. Darmofal, J. D. Kirkpatrick, V. L. DeWald, R. W. Przybylinski, G. K. Schmocker, and Y.-J. Lin, 1999: Storm reflectivity and mesocyclone evolution associated with the 15 April 1994 squall line over Kentucky and southern Indiana. *Wea. Forecasting,* **14,** 976–993.

Hamilton, R. E., 1970: Use of detailed intensity radar data in mesoscale surface analysis of the 4 July 1969 storm in Ohio. Preprints, *14th Conf. on Radar Meteorology,* Tuscon, AZ, Amer. Meteor. Soc., 339–342.

Houze, R. A., S. A. Rutledge, M. I. Biggerstaff, and B. F. Smull, 1989: Interpretation of Doppler weather radar displays of midlatitude mesoscale convective systems. *Bull. Amer. Meteor. Soc.,* **70,** 608–619.

Howieson, E. D., and G. A. Tipton, 1998: Tornadogenesis associated with the 1 July 1997 derecho—A radar perspective. Preprints, *19th Conf. on Severe Local Storms,* Minneapolis, MN, Amer. Meteor. Soc., 192–195.

Johns, R. H., 1993: Meteorological conditions associated with bow echo development in convective storms. *Wea. Forecasting,* **8,** 294–299.

——, and W. D. Hirt, 1987: Derechos: Widespread convectively induced wind-storms. *Wea. Forecasting,* **2,** 32–49.

Johnston, E. C., 1981: Mesoscale vorticity centers induced by mesoscale convective complexes. M.S. thesis, Dept. of Meteorology, University of Wisconsin—Madison, 54 pp.

Maddox, R. A., 1983: Large-scale meteorological conditions associated with midlatitude, mesoscale convective complexes. *Mon. Wea. Rev.,* **111,** 1475–1493.

Martinelli, J. T., R. W. Przybylinski, and Y.-J. Lin, 2000: Observational study of a midwestern severe wind mesoscale convective system (MCS) on 29 June 1998: A single Doppler analysis study. Preprints, *20th Conf. on Severe Local Storms,* Orlando, FL, Amer. Meteor. Soc., 382–385.

Menard, R. D., and J. M. Fritsch, 1989: A mesoscale convective complex–generated inertially stable warm core vortex. *Mon. Wea. Rev.,* **117,** 1237–1260.

NCDC, 1998: *Storm Data.* Vol. 40, No. 6, 80–83. [Available from National Climatic Data Center, 151 Patton Ave., Asheville, NC 28801-5001.]

Nolen, R. H., 1959: A radar pattern associated with tornadoes. *Bull. Amer. Meteor. Soc.,* **40,** 277–279.

Orlanksi, I., 1975: A rational subdivision of scales for atmospheric processes. *Bull. Amer. Meteor. Soc.,* **56,** 527–530.

Pence, K. J., J. T. Bradshaw, and M. W. Rose, 1998: The central Alabama tornadoes of 6 March 1996. Preprints, *19th Conf. on Severe Local Storms*, Minneapolis, MN, Amer. Meteor. Soc., 174–154.

Pfost, R. L., and A. E. Gerard, 1997: ''Bookend vortex''–induced tornadoes along the Natchez Trace. *Wea. Forecasting,* **12,** 572–580.

Przybylinski, R. W., 1988: Radar signatures with the 10 March 1986 tornado outbreak over central Indiana. Preprints, *15th Conf. on Severe Local Storms,* Baltimore, MD, Amer. Meteor. Soc., 253–256.

——, 1995: The bow echo: Observations, numerical simulations, and severe weather detection methods. *Wea. Forecasting,* **10,** 203–218.

——, and W. J. Gery, 1983: The reliability of the bow echo as an important severe weather signature. Preprints, *13th Conf. on Severe Local Storms,* Tulsa, OK, Amer. Meteor. Soc., 270–273.

——, and D. M. DeCaire, 1985: Radar signatures associated with the derecho, a type of mesoscale convective system. Preprints, *14th Conf. on Severe Local Storms,* Indianapolis, IN, Amer. Meteor. Soc., 228–231.

——, and Coauthors, 1996: Storm reflectivity and mesocyclone evolution associated with the 15 April 1994 derecho. Part I: Storm evolution over Missouri and Illinois. Preprints, *18th Conf. on Severe Local Storms,* San Francisco, CA, Amer. Meteor. Soc., 509–515.

——, G. K. Schmocker, and Y.-J. Lin, 2000: A study of storm and vortex morphology during the intensifying stage of severe wind mesoscale convective systems. Preprints, *20th Conf. on Severe Local Storms,* Orlando, FL, Amer. Meteor. Soc., 173–176.

Rotunno, R., J. B. Klemp, and M. L. Weisman, 1988: A theory for strong, long-lived squall lines. *J. Atmos. Sci.,* **45,** 463–485.

Schmocker, G. K., R. W. Przybylinski, and E. N. Rasmussen, 2000: The severe bow echo event of 14 June 1998 over the mid-Mississippi valley region: A case of vortex development near the intersection of a preexisting boundary and a convective line. Preprints, *20th Conf. on Severe Local Storms,* Orlando, FL, Amer. Meteor. Soc., 169–172.

Skamarock, W. C., M. L. Weisman, and J. B. Klemp, 1994: Three-dimensional evolution of simulated long-lived squall lines. *J. Atmos. Sci.,* **51,** 2563–2584.

——, J. B. Klemp, and J. Dudhia, 2001: Prototypes for the WRF (Weather Research and Forecasting) model. Preprints, *Ninth Conf. Mesoscale Processes,* Fort Lauderdale, FL, Amer. Meteor. Soc., J11–J15.

Smith, B. E., and J. W. Partacz, 1985: Bow-echo induced tornado at Minneapolis on 26 April 1984. Preprints, *14th Conf. on Severe Local Storms*, Indianapolis, IN, Amer. Meteor. Soc., 81–84.

Smull, B. F., and R. A. Houze Jr., 1985: A midlatitude squall line with a trailing region of stratiform rain: Radar and satellite observations. *Mon. Wea. Rev.,* **113,** 117–133.

——, and ——, 1987: Rear inflow squall lines with trailing stratiform precipitation. *Mon. Wea. Rev.,* **115,** 2869–2889.

Spoden, P. J., C. N. Jones, J. Keysor, and M. Lamm, 1998: Observations of flow structure and mesoscale circulations associated with the 5 May 1996 asymmetric derecho in the lower Ohio Valley. Preprints, *19th Conf. on Severe Local Storms,* Minneapolis, MN, Amer. Meteor. Soc., 514–517.

Tessendorf, S. A., and R. J. Trapp, 2000: On the climatological distribution of tornadoes within quasi-linear convective systems. Preprints, *20th Conf. on Severe Local Storms,* Orlando, FL, Amer. Meteor. Soc., 134–137.

Trapp, R. J., 1999: Observations of nontornadic low-level mesocyclones and attendant tornadogenesis failure during VORTEX. *Mon. Wea. Rev.,* **127,** 1693–1705.

——, and G. J. Stumpf, 2002: A reassessment of the percentage of tornadic mesocyclones. Preprints, *21st Conf. on Severe Local Storms.,* San Antonio, TX, Amer. Meteor. Soc., 198–201.

——, and M. L. Weisman, 2003: Low-level mesovortices within squall lines and bow echoes. Part II: Their genesis and implications. *Mon. Wea. Rev.,* **131,** 2804–2823.

——, E. D. Mitchell, G. A. Tipton, D. W. Effertz, A. I. Watson, D. L. Andra Jr., and M. A. Magsig, 1999: Descending and nondescending tornadic vortex signatures detected by WSR-88Ds. *Wea. Forecasting,* **14,** 625–639.

Trier, S. B., C. A. Davis, and W. C. Skamarock, 2000: Long-lived mesoconvective vortices and their environment. Part II: Induced thermodynamic destabilization in idealized simulations. *Mon. Wea. Rev.,* **128,** 3396–3412.

Wakimoto, R. M., 1983: The West Bend, Wisconsin storm of 4 April 1981: A problem in operational meteorology. *J. Appl. Meteor.,* **22,** 181–189.

——, and B. E. Martner, 1992: Observations of a Colorado tornado. Part II: Combined photogrammetric and Doppler radar analysis. *Mon. Wea. Rev.,* **120,** 522–543.

——, and H. Cai, 2000: Analysis of a nontornadic storm during VORTEX 95. *Mon. Wea. Rev.,* **128,** 565–592.

Weisman, M. L., 1993: The genesis of severe, long-lived bow echoes. *J. Atmos. Sci.,* **50,** 645–670.

——, and C. A. Davis, 1998: Mechanisms for the generation of mesoscale vortices within quasi-linear convective systems. *J. Atmos. Sci.,* **55,** 2603–2622.

——, and R. J. Trapp, 2003: Low-level mesovortices within squall lines and bow echoes: Part I: Overview and dependence on environmental shear. *Mon. Wea. Rev.,* **131,** 2779–2803.

Wolf, R. A., 2000: Characteristics of circulations associated with the 29 June 1998 derecho in eastern Iowa. Preprints, *20th Conf. on Severe Local Storms,* Orlando, FL, Amer. Meteor. Soc., 56–59.

——, 2002: Doppler radar observations of squall line tornadogenesis near the KDVN WSR-88D. Preprints, *21st Conf. on Severe Local Storms,* San Antonio, TX, Amer. Meteor. Soc., 507–510.

Wurman, J., and S. Gill, 2000: Finescale radar observations of the Dimmitt, Texas (2 June 1995), tornado. *Mon. Wea. Rev.,* **128,** 2135–2164.